

1 **ROBUST METABOLOMICS APPROACH FOR THE EVALUATION OF HUMAN EMBRYOS**  
2 **FROM IN-VITRO FERTILIZATION**

3

4 **Cecilia Beatriz Figoli<sup>1</sup>, Marcelo Garcea<sup>2</sup>, Claudio Bisioli<sup>2</sup>, Valeria Tafintseva<sup>3</sup>,**  
5 **Volha Shapaval<sup>3</sup>, Mariana Gómez Peña<sup>2</sup>, Luz Gibbons<sup>4</sup>, Fernando Althabe<sup>4</sup>,**  
6 **Osvaldo Miguel Yantorno<sup>1</sup>, Marcos Horton<sup>2</sup>, Jürgen Schmitt<sup>5</sup>, Peter Lasch<sup>6</sup>,**  
7 **Achim Kohler<sup>3\*</sup> & Alejandra Bosch<sup>1,\*</sup>**

8

9 \*corresponding authors:

10 Alejandra Bosch, E-mail: [bosch@quimica.unlp.edu.ar](mailto:bosch@quimica.unlp.edu.ar)

11 Achim Kohler, E-mail: [achim.kohler@nmbu.no](mailto:achim.kohler@nmbu.no)

12

13 <sup>1</sup>CINDEFI-CONICET, CCT La Plata, Facultad de Ciencias Exactas, UNLP, La Plata,  
14 Argentina

15

16 <sup>2</sup>PREGNA Medicina Reproductiva, Ciudad Autónoma de Buenos Aires, Argentina

17

18 <sup>3</sup>Faculty of Science and Technology, Norwegian University of Life Sciences, 1432  
19 Ås, Norway

20

21 <sup>4</sup>IECS, Instituto de Efectividad Clínica y Sanitaria, Ciudad Autónoma de Buenos  
22 Aires, Argentina

23

24 <sup>5</sup>Synthon GmbH, Schriersheim, Germany

25

26 <sup>6</sup>Centre for Biological Threats and Special Pathogens (ZBS) Proteomics and  
27 Spectroscopy" Unit, Robert Koch-Institut, Berlin, Germany.

## ABSTRACT

The identification of the most competent embryos for transfer to the uterus constitutes the main challenge of *in-vitro* fertilization (IVF). We established a metabolomic-based approach applying Fourier Transform Infrared spectroscopy (FTIR) on 130 samples of 3-days embryo culture supernatants from 26 embryos that implanted and 104 that failed. Examining the internal structure of the data by unsupervised multivariate analysis, it was observed that the supernatants of nonimplanted embryos contained highly heterogeneous spectral features. These features were overlapping with metabolic-implantation fingerprints, thus demonstrating that in establishing embryo-assessment models a one-class modelling involving only the samples with positive-implantation outcomes should be applied. Analysis of variance confirmed that the women's age (>40 years) undermined the implantation of the embryos exhibiting implantation metabolomics, and also that constituted a condition triggering embryos to express nonimplantation metabolomics. We conclude that IVF-success rates can be significantly improved if FTIR spectroscopy is used as an embryo-selection criterion.

## INTRODUCTION

Infertility—a multifactorial disorder that affects around 15% of the reproductive couples worldwide—is a markedly increasing health problem due to the postponement of parenthood<sup>1</sup>. Since the first successful *in-vitro*–fertilization (IVF) birth in 1978, more than eight million children have been born with the help of assisted-reproduction techniques<sup>2,3</sup>. Although IVF is widely used to treat infertile couples, in many instances that approach does not resolve infertility problems because of its low success rate<sup>4</sup>. Several conditions lead to implantation failure, including

reduced endometrial receptivity<sup>5,6</sup>, embryonic defects such as genetic abnormalities, the overall clinical status of the mother, faults in the embryo-transfer technique, and/or other multifactorial causes<sup>7,8</sup>. One of the most crucial steps for a successful IVF treatment is definitively the selection of a competent embryo(s) for transfer. The assessment of embryo development and morphology by light microscopy is currently the usual clinically established method for assessing embryo viability<sup>9,10</sup>. This technique constitutes a fast, easy, and affordable evaluation and has been considered as the universally accepted method of choice for embryo selection<sup>9</sup>. Nevertheless, owing to the significant interobserver variability and subjectivity reported in the literature, together with the low capability of morphologic evaluation by light microscopy in predicting the implantation rate of an embryo (*i. e.*, below 30%), that approach represents an inefficient methodology for embryo selection<sup>11–15</sup>. Alternatively, invasive methods such as the preimplantation genetic testing (PGT) used to determine the genetic profiling of embryos before implantation, involve certain risks, since biopsy might negatively influence further embryo development<sup>16–20</sup>. A noninvasive and rapid evaluation of the embryo-implantation potential before transfer therefore constitutes one of the most crucial challenges in IVF treatments.

In the last decade, metabolomics has emerged as an alternative noninvasive technology to evaluate embryo implantation potential<sup>21</sup>. Human embryos, while developing in the culture media, consume available nutrients and release metabolites, thus modifying culture supernatants. Therefore, a detailed chemical analysis of the spent supernatant of an embryo's culture medium provides information reflecting cellular metabolic activities and the overall developmental status of the embryo. The relationship between the metabolic parameters and embryo viability was reported for the first time in 1980 by Renard and collaborators<sup>22</sup>. A number of proof-of-principle

78 studies related to the chemical composition of embryo's culture supernatants and the  
79 subsequent embryo-implantation outcome reported that embryos achieving  
80 implantation were different in metabolomic profile from those that failed in  
81 implantation<sup>23,24</sup>. Two different approaches were applied in the evaluation of embryo  
82 metabolomics: a targeted and a nontargeted metabolic profiling analysis. The former  
83 involves multiplexed detection or quantification of predefined metabolites and the  
84 establishment of thresholds for those detected<sup>25</sup>. The targeted analysis is based on the  
85 hypothesis that embryonic viability is mainly associated with the concentration level  
86 of certain products released into the medium, such as those related to energy  
87 metabolism (*e. g.*, glucose, pyruvate) and/or the synthesis of extracellular products (*e.*  
88 *g.*, lactate and ammonium). In contrast, the nontargeted approach produces  
89 metabolomic fingerprints of embryos containing differing multivariate traits that  
90 provide insight into the embryo's metabolic state. The extraction of information from  
91 these complex metabolic profiles requires a further advanced multivariate data  
92 analysis.

93         Several nontargeted technologies like vibrational spectroscopy (near infrared,  
94 NIR, and mid-infrared, MIR, plus Raman spectroscopy), nuclear-magnetic resonance  
95 (NMR), and matrix-assisted laser desorption/ionization-time-of-flight mass  
96 spectrometry (MALDI-TOF) of culture supernatants can provide a complete picture  
97 of an embryo's metabolism and genetic-expression patterns. Therefore, these  
98 methodologies have been broadly applied for the evaluation of embryo  
99 metabolomics<sup>26</sup>. From 2007 to 2013 studies on metabolomics profiling in spent  
100 culture media and the subsequent embryo viability were carried out through the use of  
101 different spectroscopy-based technologies<sup>23,27–33</sup>. NIR technologies combined with  
102 supervised mathematical models were established to estimate the reproductive

potential of embryos<sup>23,27–33</sup>. Different fertility centers were included in those trials, with the number of recruited patients ranging from 30 to 417. Nevertheless, none of those NIR-based metabolomics models were able to improve clinical-pregnancy rates when compared to the results obtained analyzing embryonic morphology by light microscopy<sup>28,29,31</sup>. In addition, a preliminary MIR-spectroscopy assay demonstrated the great potential of Fourier-transform–infrared (FTIR) spectroscopy in the screening of the embryonic-implantation potential. Only 7 samples of 26-hour–embryo-culture supernatants from 5 patients were studied, however; and no additional publications with larger cohorts of patients have appeared so far<sup>34</sup>. Finally, Bracewell-Milnes and collaborators (2017), reviewing the potential of the metabolomic technologies as applied to IVF, concluded that the metabolomic profiling of embryo supernatants, as studied up to date, has not evidenced any improvement in the prediction of embryonic viability in clinical practice<sup>26</sup>.

FTIR spectroscopy is a noninvasive analytical physicochemical technique providing information about the total biochemical composition of the analyzed material and has the remarkable advantage of involving a straightforward form of sample preparation and a short spectral-data–acquisition time. FTIR spectroscopy has been successfully used as an analytical tool in a wide range of fields including food, biotechnology, and microbiological and medical diagnostics<sup>35,36,45,37–44</sup>. The potential of FTIR-analysis of blood components (*e. g.*, serum, plasma) and other biofluids (*e. g.*, bile, urine, sputum) for diagnostic purposes has been widely investigated and recognized<sup>46–54</sup>. The great ability of this spectroscopy technology to detect small changes in different types of samples has led to its application in other fields such as the study of extracellular and intracellular metabolites in bacterial<sup>40</sup>, fungal<sup>55</sup>, and mammalian-cell cultures<sup>38,39</sup>. In particular, glucose, glycerol, and acetic acid were

measured in *Escherichia coli* cultures<sup>40</sup>, while glucose and lactate concentrations were evaluated in mammalian-cell lines<sup>38</sup>.

From the aforementioned results, we can conclude that the application of vibrational spectroscopy as a diagnostic and prognostic tool has the potential to thoroughly change the assessment of the traditional clinical systems that improve patients healthcare and in so doing enhance the efficiency of the health services<sup>56</sup>. The development of novel technologies for spectral measurement and data analysis increases the possibilities of applying these sophisticated spectroscopic methodologies to routine clinical diagnoses<sup>57</sup>.

In view of this strong background, the aim of the present study was to test FTIR spectroscopy combined with multivariate data analysis as a means for a noninvasive assessment of human-embryo metabolomics. For this purpose we characterized 3-day-embryo–culture supernatants by FTIR spectroscopy and evaluated whether changes in the infrared patterns could be associated with the outcome of IVF. Since implantation is a highly complex multifactorial process, we also considered different clinical features with potential impact on implantation rates.

## RESULTS

**A robust FTIR experimental approach for metabolomic analysis of 3-day-embryo–culture supernatants.** In the development of a novel method for the evaluation and selection of embryo-implantation potential based on FTIR vibrational spectroscopy, we established a 3-h protocol for sample preparation and spectral acquisition (Fig. 1). The protocol stated in brief: Supernatants are recovered from individual embryo cultures and centrifuged to remove the culture oil. Then 30  $\mu$ L are transferred to a 96-multiwell ZnSe optical plate. Next, the samples are dried under

moderate vacuum (0.1 bar) for 45 min until transparent films are obtained<sup>52,58</sup>. Finally, FTIR transmission-type measurements are carried out in the spectral range 650–4000 cm<sup>-1</sup> at a 6-cm<sup>-1</sup> spectral resolution.

Because FTIR is an extremely sensitive analytical technique, a strict reproducibility analysis was performed to assure the construction of a robust infrared spectral database for further data analysis (Methods). We studied the reproducibility among the measurements obtained for the 96 positions of the ZnSe optical plate using the same batch of fresh culture medium. This analysis demonstrated that the spectral quality was not affected by the desiccation of the samples observed during the lengthy time required for the measurement of 96 samples (Supplementary Fig. 1). A high level of reproducibility was also observed among the samples from each batch and among different batches of G1 Plus culture medium (Supplementary Figs. 2 and 3).

**FTIR spectral characterization of spent embryo-culture medium.** Fig. 2, Panel a, depicts a representative and exemplary FTIR absorption spectrum of a 3-day-embryo-culture supernatant recovered from a successfully implanted embryo (class IMP in this study), while Fig. 2, Panel b lists the assigned spectral bands and their respective functional groups. The main spectral windows (W1–W5) associated with the molecular building blocks of complex biologic samples<sup>58</sup> could be identified: The spectral region associated preferentially with lipids (W1) between 2800 and 3000 cm<sup>-1</sup> exhibits bands assigned to the symmetric and antisymmetric C–H stretching modes of methyl groups (–CH<sub>3</sub>) detected at 2874 and 2969 cm<sup>-1</sup>, respectively; and the antisymmetric C–H stretching mode for methylene residues (>CH<sub>2</sub>) at 2933 cm<sup>-1</sup>. The infrared spectral region associated with protein absorptions (W2) evidenced the typical amide-I and amide-II bands at 1655 and 1545 cm<sup>-1</sup>, respectively. The mixed



region (W3) between 1200 and 1500  $\text{cm}^{-1}$  represents absorptions of stretching and bending vibrations from fatty acids, polysaccharides, nucleic acids, and proteins. A characteristic band is observed around 1400  $\text{cm}^{-1}$ , which absorbance may be attributed to the symmetric stretching vibrations of the  $-\text{COO}^-$  functional groups of amino-acid side chains or free fatty acids. In this region, a typical amide-III band at 1315  $\text{cm}^{-1}$  was also observed along with bands of different  $>\text{P}=\text{O}$  asymmetric stretching at around 1230  $\text{cm}^{-1}$ . The vibrational modes of the carbohydrate region (W4) between 900 and 1200  $\text{cm}^{-1}$  is generally dominated by the symmetric stretching vibration of  $\text{PO}_2^-$  groups (1090  $\text{cm}^{-1}$ ) in nucleic acids and a complex sequence of peaks mainly due to the C–O–C and C–O–P stretching vibrations of various oligo- and polysaccharides<sup>58</sup>. That region also contains bands assigned to the C–O stretching vibrations in carboxylic groups—*e. g.*, in lactate at 1041  $\text{cm}^{-1}$  and 1120  $\text{cm}^{-1}$ <sup>59,60</sup>. Finally, the region between 650 and 900  $\text{cm}^{-1}$  (W5) contains weakly expressed bands arising from the aromatic-ring vibrations of phenylalanine, tyrosine, tryptophan, and the various nucleotides. With the exception of only a few peaks (*e. g.*, a band near 720  $\text{cm}^{-1}$ , resulting from the  $>\text{CH}_2$ -rocking modes of the fatty-acid chains), valid assignments can hardly be achieved. W5 exhibits a variety of extremely characteristic, features superimposed on an underlying broad spectral contour. Therefore, we refer to this spectral domain as the true fingerprint region<sup>58</sup>.

**Development of a predictive embryo-implantation model based on the FTIR metabolomic profile of embryo supernatants.** The internal structure of the spectral data was studied by the unsupervised multivariate method of principal component analysis (PCA). This analysis aims at transforming the original variables, which here referred to wavenumbers in infrared spectroscopy, into smaller numbers of new

variables or principal components that describe the main variation patterns<sup>61</sup>. The PCA-score plot obtained (Fig. 3, Panel a) revealed that the spectral fingerprints of the supernatants from the implanted embryos (IMP, black squares) were quite similar among themselves and formed a relatively homogeneous cluster in the principal-component space (Supplementary Note 1 and Supplementary Fig. 4). In contrast, the spectra recorded from the supernatants of nonimplanted embryos (class NIMP, green squares) were distributed over a much wider range, thus exhibiting a larger spectral heterogeneity (see Supplementary Note 1 and Supplementary Fig. 4). Of interest to us was that the coordinates of the IMP and NIMP patterns completely overlapped. This observation and the higher heterogeneity level of NIMP fingerprints, suggested the presence of altered metabolic states in the embryos that did not implant. We were tempted to speculate that some of those altered states may be responsible for the nonimplantation. Within this context, we also need to mention, however, that a significant fraction of spectral fingerprints from the nonimplanted embryos (NIMP) proved indistinguishable from the supernatants of the implanted embryos (IMP, *cf.* the overlap in Fig. 3, Panel a). This finding would be in accord with our working hypothesis that certain embryos, though expressing the metabolomic biomarkers for embryo implantation, failed to implant for other reasons. Some of those conditions influencing implantation outcome that are not associated with metabolomics could be *e. g.*, maternal features like overweight, age, and smoking habits, among others.

To test our hypothesis, we employed the method of soft independent modelling of class analogies (SIMCA)<sup>62</sup>, a one-class modelling technique that involves only a single class of objects to establish a discrimination model. The model can then be used to classify any new subject as to either belonging to the class or

228 being outside of the class. This approach is particularly well suited in the example of  
229 embryo-supernatant data since embryos with implantation results (IMP) are quite  
230 similar among themselves and can be used to establish such a model, whereas the  
231 embryos with nonimplantation results (NIMP) are more disparate. Thus, a SIMCA  
232 model was established with the spectra of IMP group. The SIMCA model is  
233 represented by a class border (see Fig. 3, Panel b, curved line) that separates samples  
234 that belong to the class} from those falling outside the class. The model then, upon  
235 challenge by the NIMP samples, separated that class into two groups. The first  
236 contained the so-called "implantation fingerprints" (IF)—*i. e.*, comprising spectra  
237 from samples with a metabolic fingerprint similar to IMP (Fig 3, Panel b, orange  
238 dots). The second class, formed by putative "nonimplantation fingerprints" (NIF),  
239 contained spectra from supernatants with altered metabolic states (Fig 3, Panel b, blue  
240 dots). We need to note here that the NIMP spectra exclusively—but no IMP  
241 samples—are plotted in Fig. 3, Panel b. Therefore, from this plot we can clearly  
242 recognize that some NIMP fingerprints belong to the model space characterized by  
243 implanted-embryo fingerprints (IF, orange dots) while others fall outside that model  
244 space (NIF, blue dots). This situation is also reflected in the logic diagram in Fig. 3,  
245 Panel c; which representation illustrates that the class IF was composed of all 26 of  
246 the IMP spectra along with 40 of the NIMP spectra having features of the metabolic-  
247 implantation fingerprint (the 40 orange dots in Fig. 3, Panel b), all together totalling  
248 66 samples. The NIF class contained the remaining 64 fingerprints from NIMP  
249 spectra (blue dots in Fig. 3, Panel b). What was also of interest was that the  
250 classification by the SIMCA model provided an almost perfect balance between the IF  
251 and NIF classes (*i. e.*, 66 *versus* 64). This observation suggested that, according to our  
252 hypothesis, roughly half of the embryos had implantation potential.

An in-depth analysis of the second derivatives of spectra belonging to NIF and IF groups revealed certain spectral differences mainly in the spectral bands associated with amino acids and carbohydrates located within W2 and W4, respectively (Fig. 2). Indeed, a decrease in the intensities of the 1590 and 1530  $\text{cm}^{-1}$  peaks were observed in IF in comparison with those of the NIF spectra (Supplementary Fig. 5). This result could be indicative of a difference in the amino-acid turnover between the two groups of embryos. Furthermore, in the spectral regions associated with the lactate-group absorption bands (at 1120 and 1041  $\text{cm}^{-1}$ ), the IF spectra exhibited more intensive peaks than did the NIF, which difference might represent a higher lactate production due to an increase in glucose uptake in the embryos of the IF group<sup>59,63</sup>. These results also revealed that SIMCA analysis could in fact discriminate between embryos presenting different metabolomic profiles.

To support this hypothesis—and with an aim at identifying potential causes for the embryos with implanting metabolomic fingerprints (IF class) to have failed to implant—different statistical analyses were performed. For this purpose we used the patients' clinical data registered in the OpenClinica database (*cf.* the methods section). This database contained certain patient parameters that are known to be associated with implantation outcomes such as women's age (between 27 to 42 years classified in three categories, <35, from 35 to 40, and >40), women's body-mass index ([BMI], divided into 4 classes from normal weight to obesity), and smoking habits (categorized in 5 groups, from nonsmoker to smoker at more than 20 cigarettes per day). Each of these parameters was analyzed independently (one-way analysis of variance [ANOVA]) and in combination (multivariate analysis of variance [MANOVA]). Through this approach, we could confirm that the woman's age was the main factor significantly associated ( $p < 0.05$ ) with the nonimplantation of embryos

within the class NIMP classified by SIMCA as the IF class (comprising those having implantation potential; Supplementary Fig. 6, Panel a). Accordingly, upon analyzing the distribution of the mothers' ages, we found that within the IF class the IMP group (those same 26 samples) did not contain women older than 40 years, while the NIMP group (40 samples) included women of all three age-categories (age groups 1, 2 and 3; Supplementary Fig. 7, Panel a). Furthermore, we searched if any of the external parameters analyzed here could have triggered the embryos to express either IF or NIF metabolomics. In an ANOVA comparison between the classes IF (26 + 40 samples) and NIF (64 samples), we found that the samples predicted as NIF were typical of women of a statistically relevant higher age (Supplementary Fig 6, Panel b). In fact, a comparison of the distribution of the mothers' ages within IF and NIF revealed that the NIF class contained a higher number of women older than 40 years (Supplementary Fig. 7, Panel b).

In view of the morphology grade of the embryos as assessed by the Istanbul-consensus criteria<sup>9</sup>, a statistical analysis ( $\chi^2$ ) demonstrated that the morphologic distribution of the embryos (grades 1, 2, and 3) observed within the IF and the NIF classes was also not significantly different (Fig. 3, Panel d,  $p = 0.125$ ). Therefore, a grading system based on the embryo-cleavage rate and morphologic features were found not to be correlated with the different metabolomic patterns obtained by FTIR spectroscopy.

At this juncture, we would like to point out some fundamental pragmatic considerations. If FTIR spectroscopy is to be used in a practical arrangement as a method for identifying embryo candidates suitable for implantation, only embryos with the metabolic implantation-fingerprint class IF would be considered, while embryos of class NIF would be disregarded. Under these conditions, the success rate

of implantation in the present study would have equaled ~40%. This value can be obtained by the formula  $IMP/IF = 26/(26 + 40) = 39.4\%$ . In contrast to such an application, however, the present study employed FTIR spectroscopy only retrospectively after the implantations had been performed. As a consequence, all 64 embryos of the NIF class were transferred because those embryos had met all the morphologic criteria for successful implantation. The success rate in this instance—*i. e.*, without application of the FTIR criteria—was only 20% [ $IMP/(IMP + NIMP) = 26/(26 + 40 + 64)$ ]. Thus, the success rate achievable with FTIR spectroscopy would have been almost twice as high as the rate of embryo assessment without considering the FTIR criteria. Of course, this retrospective data would need to be carefully reviewed and validated in a larger study. Nevertheless, this example clearly argues that the metabolomic criteria developed in our study have the potential to significantly improve the success rate of embryo implantation.

## DISCUSSION

Assisted-reproduction techniques (ART) are globally adopted methods that occupy a central place in reproductive medicine. IVF in particular, enhances the possibility of pregnancy and also enables women to conceive in situations which would not have been possible decades ago<sup>64</sup>. Nevertheless, the success rate of that reproductive treatment is still low (only 30%). Although depending on many different parameters<sup>54</sup>, the crucial step of the process is clearly the selection of a fully competent embryo for transfer. Accordingly, obtaining and selecting an embryo with the highest implantation potential is still the key objective within the state of the art in IVF laboratories. Different techniques based on diverse approaches for embryo assessment—*e. g.*, morphokinetics, genetics, proteomics, metabolomics—are

constantly being proposed. Among noninvasive metabolomic-based techniques, NIR spectroscopy has represented a widespread analytical technique for carrying out a direct study of embryo supernatants. That approach offers a wide diversity of instrumentation available today, provides the possibility of using portable on-field spectrometers, and further supernatant spectra can be directly measured owing to the limited water interference<sup>65-67</sup>. NIR technology produces very wide bands due to the absorption of few signals from the molecular overtones along with a combination of stretching-bending vibrations of atomic groups such as O-H, C-H, and N-H<sup>67</sup>. The group of Dr. Denny Sakkas at the University of Massachusetts, Boston developed an NIR-based technique combined with supervised mathematical models for embryo selection and applied that procedure to different cohorts of patients. That strategy, however, was unable to further improve pregnancy rates, even when combined with an evaluation of embryo morphology<sup>23,28,29,31-33,68</sup>. In contrast, MIR spectroscopy provides much more information about the biochemical composition of the biologic materials<sup>58</sup>. MIR spectra arise from the stretching and bending vibrations resulting from all bonds that exhibit a transition dipole moment, such as C-H, C=O, C-O, O-H, N-H, C-N, among others. FTIR spectroscopy is hence more sensitive than NIR to the full range of biomolecules present in biologic samples, and even more so when the dried-film technology is applied to guarantee that the strong features of water-absorption bands, which interfere in the spectrum, are avoided<sup>54,56,58,69</sup>.

In its current state, the NIR technique provides no clinical benefit. Nevertheless we are convinced that the main reason for its low success is not only due to limitations in the spectroscopy technology itself, but also to the data structuring (data classification), and the analytical approaches used for the data analysis. In most of those investigations the available data were first organized in two classes: i)

353 samples belonging to embryos that implanted or resulted in a live birth and ii) samples  
354 belonging to embryos that failed to do either. Then, these two classes served as  
355 reference data for training different supervised learning algorithms<sup>54,58</sup>. Supervised  
356 data-processing methods such as genetic algorithms, or least-squares regressions use  
357 the spectra *a priori* assigned to classes, as teaching information to build models that  
358 are later used to predict the outcome of unknown samples. Our great concern at this  
359 point is that we demonstrated here that nonimplanted-embryo supernatants (the  
360 NIMPs) do not follow any specific pattern. Quite the contrary, these embryos  
361 represent a highly heterogeneous group of spectra (Fig. 3, Panel a, Supplementary  
362 Note 1, and Supplementary Fig. 4). Moreover, among the NIMP group of samples, a  
363 significant number might belong to embryos that could be good candidates on the  
364 basis of their metabolomic patterns having biochemical-implantation fingerprints  
365 similar to those of the implanted embryos, but failing to implant owing to the other  
366 parameters not associated with metabolomics and thus not reflected in spectroscopic  
367 methods (*e. g.*, the maternal age for example; Supplementary Figs. 6, Panel a and 7,  
368 Panel a). Those samples were therefore falsely grouped in the wrong class from the  
369 metabolomics point of view. Consequently, the use of the fingerprints of  
370 nonimplanted embryos as one of the references on which to establish an implantation  
371 model disregards the reality that implantation is multifactorial.

372         We need to underscore that in most of the investigations based on molecular  
373 methods such as genomics, transcriptomics, or proteomics for embryo-viability-  
374 assessment, the data were first preclassified according to implantation outcomes, and  
375 supervised models were subsequently formulated with the information contained in  
376 both implantation and nonimplantation classes as reference data<sup>23,27–32,34</sup>. Our study  
377 presents a completely novel approach for classifying the samples according to their



implantation potential and reveals the underlying reasons for the differences between the implantation and nonimplantation of samples. In the results reported here, we demonstrated that classification models should be established differently from the existing models within the field. We established our classification model using the data of implanted embryos (IMP) in a one-class modelling technique called SIMCA. Utilizing the information of the class with known and homogenous properties (IMP in this study), we were able to predict whether a new sample belonged to the defined class or not. The other class might have a much larger variation that is partially unknown. This approach is highly relevant to the present study since we might encounter an embryo with a different metabolic fingerprint that was not accounted for in the existing sample set. Upon applying SIMCA modeling, the IMP and NIMP groups become redefined into two new classes according to the implantation fingerprint (IF and NIF; Fig. 3, panels b and c).

With respect to our SIMCA model, many embryos presenting metabolomic implantation-fingerprints did not implant (40 NIMP embryos included in the IF group, Fig. 3, Panel c). Thus, those embryos did not implant even though they had an implantation potential according to our model. The successful implantation of an embryo relies on intricate and multiple contributions—not only from eggs and sperm, which determine the quality of resulting embryos—but also from the endometrium, ovarian-stimulation regimes, laboratory conditions, and many external parameters<sup>70</sup>. We indeed were able to demonstrate that those NIMP embryos with metabolomic implantation fingerprinting IF (40 samples in Fig. 3, Panel c) did not implant because of the multifactorial nature of the outcome in pregnancy. An ANOVA analysis of the patients' data recovered in this study (maternal age, BMI, smoking habits), revealed

that maternal age represented at least one of those causes for nonimplantation of these NIMP-IF embryos.

Another question that we could address was if external parameters could negatively influence embryos to express either an implantation metabolomics or a nonimplantation metabolomics. Again, we found that the maternal-age distribution was at least one of the features that differentiated embryos IF from NIF (Supplementary Fig. 6, Panel b and Fig. 7, Panel b). That the strongest influence related to a woman's chance to become pregnant is her age is well known<sup>71-77</sup>; with advanced age causing a reduction in the ovarian follicular pool, perturbations in ovulation, and an increase in meiotic errors within the oocyte<sup>64,78</sup>. This is one among several different clinical predispositions that could induce an embryo to express an implantation or nonimplantation metabolomic fingerprint. To the best of our knowledge, the present study is the first to combine embryo-metabolomic data with patient clinical features.

Different strategies can be described for the process of selecting the embryo with the highest probability of implantation within an embryo cohort. The first represents the development of models that identify embryo biomarkers associated with embryo "quality". In this regard, we can apply different approaches—namely, those based on embryonic morphology (microscopic morphologic analysis, time-lapse imaging techniques), on the quality of the embryo's genetic material (noninvasive PGT), or on embryo metabolomics (NIR, FTIR, Raman, proteomics methods). Then, if a large cohort of patients were available, by combining more than one of these different approaches to assess embryonic viability, a further improvement in developing robust multifactorial implantation models for selecting of the best embryo for transfer would also be possible. Nevertheless, even then, we still could not ensure

that such embryos with the best “score” would implant. We have demonstrated here that suitable candidates from the metabolomic point of view, may fail in their implantation owing to other parameters, of equal consequence, associated with patients’ life-style, habits, and/or external characteristics such as smoking habits, BMI, age, stress—in addition to the embryo-transfer quality—just to mention a few. Consequently, a margin of uncertainty involving the patients’ profile and external conditions will always exists, which elements are often difficult to include in a model. Therefore, our present experience would dictate that, to enhance the efficiency of IVF procedures, efforts should focus particularly on two aspects i) combining different approaches for embryo assessment (morphokinetics, genetics, proteomics, metabolomics), and ii) improving data treatment. The combination of different embryo-assessment methods could enable the evaluation of an embryo's complete status with respect to implantation outcome. This multimodal approach could then improve the possibilities for embryologists to select embryos with the highest implantation potential.

In this work, we have demonstrated for the first time the potential of FTIR spectroscopy combined with multivariate analysis for gaining insights into fundamental aspects associated with embryo metabolomics and for improving implantation outcomes. In a retrospective analysis examining the combined results of FTIR and SIMCA, we observed that within the NIMP group more than 50% (64 out of 104 embryos) presented an NIF pattern (Fig. 3, Panel c). Thus, these NIMP-NIF embryos would not have been transferred to mothers if they had first been analyzed by the approach employing both FTIR and SIMCA. We need, however, to remark that the criterion for selecting the embryos for transfer was based largely on their morphologic appearance (86% of these embryos presented the highest morphology

grade according to the Istanbul consensus). Therefore, our results indicate that a reconstruction of the data including SIMCA in the IF and NIF will certainly be helpful as a practical adjunct since this additional information would decrease the failure rates and significantly improve the overall IVF outcome. Nonetheless, these results definitely have to be verified experimentally in a follow-up study.

In conclusion, this work has established the basis for how embryo data should be analyzed in order to develop new models for embryo selection in IVF treatments. This research therefore constitutes a significant contribution in the area of assisted fertilization, by offering a novel approach for embryo assessment in IVF treatments and revealing the cause of the failure to establish a reliable metabolomics-based model to predict embryo-implantation outcome.

## **MATERIALS AND METHODS**

**Ethical approval.** Participants were recruited and provided written consent according to Section IRB00001745-IORG 0001315 of the protocols approved by a national ethics committee for medical education and clinical research [Centro de Educación Médica e Investigaciones Clínicas Norberto Quirno (CEMIC), Argentina].

**Patients.** The patients participating in the study were recruited from the fertility center “PREGNA-Medicina Reproductiva”, Buenos Aires, Argentina, during the period from October 2012 through December 2015.

All women below 42 years old treated at PREGNA and undergoing IVF treatments were considered for participation in the study, but patients with more than two previous IVF attempts were excluded. The diagnosis of the cause of female or male infertility, the protocol applied for ovarian-stimulation, and whether the

conventional IVF or an intracytoplasmic sperm injection was employed were not considered as exclusion criteria. The stimulation protocols consisted of the application of gonadotropins and the gonadotrophin-releasing-hormone antagonist in combination with recombinant and/or highly purified urinary gonadotropins.

**Embryo culture.** Upon oocyte retrieval, cumulus-oocyte complexes were placed in four-well plates containing 500 µL of G-IVF Plus medium covered with mineral oil (OVOIL-Culture Oil) to avoid evaporation (all the culture media used in this study were from Vitrolife, Göteborg, Sweden). In parallel, semen samples were processed through discontinuous 90–50% density gradients (Spermgrad) and double washed in sperm preparation medium. The sperm suspension was adjusted to 200.000 motile sperm/mL in that medium and kept at room temperature (20–23 °C) until insemination. For conventional IVF, insemination was carried out 4 h after oocyte retrieval in the G-IVF Plus culture medium. For intracytoplasmic sperm injection, cumulus cells and the corona radiata of oocytes were removed by a brief exposure to 80 IU/mL of hyaluronidase (Hyase-10X) 3–4 h after collection. This fertilization procedure was performed according to the standard protocol<sup>79,80</sup>.

After 18–20 h postinsemination, the fertilization was checked and two pronuclei-stage embryos were cultured individually in 40-µL droplets of overnight-equilibrated G-1 Plus medium covered with culture oil in an IVF Tri-gas Incubator Model G185 (K-Systems, Birkerød, Denmark). For each cohort of embryos a drop of G1 Plus medium was incubated under the same conditions as a control.

Embryos incubated for 3 days were individually observed by optical microscopy for morphological grading according to the Istanbul-consensus criteria (European Society of Human Reproduction and Embryology and the Alpha Scientists'

Special-Interest Group)<sup>9</sup>. The embryos were classified as grade 1 (good quality), grade 2 (fair quality), grade 3 (poor quality) and grade 4 (arrested or undeveloped).

The highest-quality embryos from each cohort (one or two) were selected to be transferred. All the single embryos were retrieved from their supernatants. In all instances, only fresh embryos were transferred as described elsewhere after placing them in G-2 Plus culture medium<sup>81</sup>. Spent supernatants, drops of control culture media, samples of different batches of the G-1 Plus culture medium, and samples of the culture oil used were registered and stored under liquid nitrogen for further FTIR spectral analysis.

**FTIR spectroscopic analysis.** The dried-film FTIR technology<sup>54,56,58,69</sup> was applied to analyze the 3-day-embryo–culture supernatants. For this purpose, a protocol for sample preparation was optimized. Cryopreserved supernatants were thawed at room temperature (25 °C) and centrifuged for 5 min at 1690 x *g* to separate possible remnants of the culture oil in the samples. Different volumes of supernatants (15, 20, and 30 µL) were then pipetted onto each well of a ZnSe 96-well microtiter plate. The samples were dried under moderate vacuum (0.1 bar) or until transparent films were formed<sup>52,58</sup>. FTIR absorption spectra were measured in a Vertex 70 FTIR spectrometer coupled to the high-throughput HTS-XT automatic module under dried-air circulation (Bruker Optics GmbH, Ettlingen, Germany). The spectra were recorded in the transmission mode within the spectral range between 650 and 4000 cm<sup>-1</sup> with a 6 cm<sup>-1</sup> spectral resolution by taking 64 scans that were subsequently averaged. Before each sample measurement, background spectra of the ZnSe substrate were collected in order to account for variation in water vapor and CO<sub>2</sub>, with OPUS spectroscopy software (version 7.0; Bruker Optics GmbH, Ettlingen, Germany) being used for

automatic spectral acquisition. The FTIR spectra of both, the different batches of the culture medium and of the culture oil, used for the different reproducibility studies here performed, were likewise measured according to the procedure described above.

**Data analysis.** The data-analysis flow sheet applied in this study was specifically developed for the optimized processing of embryo-supernatant FTIR spectra and comprised the following routines: 1) data preprocessing, 2) construction of the FTIR database, 3) hierarchical-cluster analysis (HCA), 4) principal-component analysis (PCA), 5) soft independent modelling of class analogy (SIMCA), and 6) statistical analysis (Fig. 4).

Data pretreatment. In order to increase the quality of the FTIR spectral features, to reduce interference from noise, and to avoid interfering signals from water vapor and culture oil that could mask the spectral biomarkers specifically associated with implantation; a spectral preprocessing was applied<sup>82</sup>. As a first step, all raw spectra were subjected to a quality test of our own design through the use of OPUS-spectroscopy software 7.0 (Bruker Optics, Ettlingen, Germany). This test involved checking the following parameters: (i) absorbance in the amide I region (1600–1700  $\text{cm}^{-1}$ ) with acceptable values being between 0.125 and 1.20 absorbance units, (ii) the signal-to-noise ratio (calculated from the first derivatives of the spectra between 2000 and 2100  $\text{cm}^{-1}$ ) with admissible values being lower than  $1.5 \times 10^{-4}$  and, (iii) water-vapor content (determined from the first derivatives of the absorbance values between 1837 and 1847  $\text{cm}^{-1}$ ) with acceptable values being lower than  $3 \times 10^{-4}$ <sup>52,58</sup>. Because of small quantities of culture oil that were always left in the supernatants after the centrifugation, which could further interfere with FTIR spectral signals; an additional parameter in the quality test, the so-called “ $\lambda$ ”, was defined. Parameter  $\lambda$  indicates the

level of contamination of the supernatant with the culture oil in the infrared-  
absorbance spectra as follows: the ratio of the intensity of the peak at  $2933\text{ cm}^{-1}$   
assigned as C–H stretching of  $>\text{CH}_2$  groups (lipids)—used as a marker band of oil  
content ( $I_{2933}$ )—and the intensity of the peak at  $1655\text{ cm}^{-1}$  assigned to amide I—used  
as an internal standard of the total biomass ( $I_{1655}$ , where  $\lambda = I_{2933}/I_{1655}$ ; Supplementary  
Fig. 8). Only spectra with  $\lambda \leq 0.33$  were included in the FTIR database.

For spectra that passed the quality test two different types of spectral  
preprocessing were developed: one for technical-reproducibility analysis which was  
applied among i) the different wells of the ZnSe optical plate, ii) the samples of the  
different culture medium batches, and iii) the samples recovered within each culture  
medium batch. Another preprocessing was applied to the spectra of supernatant  
samples before the PCA and SIMCA analyses. In the first, the so-called preprocessing  
A, spectra were preprocessed by calculating the second derivative (Savitzky-Golay, 17  
windows size) in the regions  $2800\text{--}3000$ ,  $1500\text{--}1800$ ,  $1250\text{--}1500$  and  $900\text{--}1200\text{ cm}^{-1}$ ;  
in the second, the so-called preprocessing B, data were preprocessed by taking the  
second derivatives (Savitzky-Golay, 3rd-degree polynomial, 17 windows size) in the  
regions  $1500\text{--}1800$ , and  $730\text{--}1280\text{ cm}^{-1}$ , with extended multiplicative signal  
correction (EMSC) applying linear term<sup>61</sup>.

These spectral-preprocessing approaches enabled an increase in the resolution  
and a more facile interpretation of the spectra along with the detection and removal of  
outliers. Higher robustness and improved accuracy in subsequent classifications and  
quantitative analyses are therefore achieved<sup>52,58,82,83</sup>.

Construction of the FTIR database. To facilitate the subsequent data analysis, an FTIR  
spectral library was developed containing normalized derivative spectra of 1) spent  
supernatants, 2) samples from different batches of the culture medium G-1 Plus, and



3) samples from the culture oil used during the study. All the spectra and the corresponding normalized derivatives were classified in two groups (Fig. 5). *Group A* comprised spectra of control samples: culture media, different batches of the culture medium G-1 Plus, and the culture oil. *Group B* consisted of spectra of the supernatants of the embryos that were transferred to the patients, with the IMP group constituting the spectra of supernatants from embryos that implanted (100% implantation), and the NIMP group the spectra of supernatants from nonimplanting embryo (0% implantation).

The supernatant spectra of the group IMP pertained to embryos whose morphologies were 30.8% grade 1 and 69.2% grade 2, where embryos of grade 3 were not found, whereas the supernatants of the NIMP group contained 33.7%, 50.0%, and 16.4% of embryos with morphologies of grades 1, 2, and 3, respectively.

Hierarchical cluster analysis (HCA). This unsupervised-analysis technique was used for checking the reproducibility of the measurements and to detect outliers in the data sets<sup>46</sup>. As previously reported<sup>52,84,85</sup>, the spectral variances in the data were determined as the average  $\pm$  2 standard deviations of the so-called spectral distance (D). This parameter corresponds to a dissimilarity measurement equal to  $(1 - r) \times 1000$ , with  $r$  being Pearson's product-moment–correlation coefficient. For estimating the reproducibility of measurements among samples within the same batch and among different batches of G1 Plus culture medium, the spectral distances were calculated by using the preprocessing procedure A (*cf.* Section Data pretreatment; Supplementary Figs. 1–3). The fusion values in dendrograms were obtained by using the average linkage (OPUS versions 7.0 Bruker Optics GmbH, Ettlingen, Germany).

Principal Component Analysis (PCA). To study the underlying pattern in the data, a PCA analysis of the FTIR metabolomic fingerprints of the 3-day-embryo supernatants

was performed. For this purpose the data were analyzed by applying the preprocessing procedure *B* (*cf.* Section Data pretreatment). This analysis was carried out by using Matlab-based in-house algorithms (Matlab R2019a, The MathWorks Inc., Natick, MA).

Soft independent modelling of class analogy (SIMCA). For separating the embryo supernatant with implantation-fingerprint spectra from those with nonimplantation spectral fingerprints, the SIMCA<sup>62</sup> pattern-recognition method was employed. The model was established by using class-IMP data only. The spectra were preprocessed by the procedure *B* (*cf.* Section Data pretreatment). To perform SIMCA analysis the Matlab GUI tool DD-SIMCA was used<sup>86</sup>. SIMCA relies on PCA and enables the creation of a border—a hyperplane—around a class of objects (class IMP in this instance) with the type of confidence interval that can be constructed by using different significance levels. The number of components for the PCA model was fixed to 3 and corresponds to a ~90% explained variance. The significance level was set at 0.01. After the model was established, preprocessed spectra from the class NIMP (nonimplanted embryo spectra) were used to discriminate embryos that fell within the model's borders (*i. e.*, with an IF-class implantation fingerprint in this instance) from those outside that model exhibiting no implantation fingerprints (the NIF class).

Statistical analysis. An ANOVA was performed on the maternal metadata, with the IF class being considered separately, and on the IF *versus* the NIF class obtained by SIMCA modelling. Different parameters such as the maternal age, body-mass index (BMI), and smoking habits were analyzed as a single parameter both separately by ANOVA and all together by the MANOVA.

Chi<sup>2</sup> analysis was performed to evaluate the embryo distribution within the IF and NIF classes.

**Construction of a database platform for research-data management—**

**“OpenClinica”.** This research was performed under strict international biosafety regulations, applying the "Best Practices for Research Data Management". For this purpose, we used an open-source software OpenClinica, based on electronic forms and protocols for storage, classification, analysis, and data visualization<sup>87</sup>. For the construction of this database, information was registered such as the patients' personal details, hormonal treatments, embryo morphology, pregnancy outcome, and results from the quality tests of the acquired spectra. This platform is currently operating effectively on the web site <https://www.openclinica.com/>. The data registered at the OpenClinica database like the mother's age, BMI, and smoking habits were converted from numerical variables into qualitative ones.

The mother's age was categorized in 3 groups: Group 1, women older than 27 and younger than 35 years; Group 2, women between 35 and 40 years; and Group 3, women older than 40 years.

The BMI was calculated in each individual by using the patient's height and weight information in the formula  $(\text{weight in kg})/(\text{height in m})^2$  and then classified into 4 groups. Those patients with BMI values between 18.5 to 25.0 (normal weight), were included in Group 1, BMI values below 18.5 (underweight) were placed in Group 2, BMI values between 25.0 to 30.0 (overweight) corresponded to Group 3, and those with BMI values over 30.0 (obesity) were categorized in Group 4.

The information related to smoking habit provided by the mothers was divided into 5 categories: Group zero (0), women that never smoked; Group 1, ex-smokers that used to consume fewer than 10 cigarettes per day; Group 2, ex-smokers that used to smoke more than 10 cigarettes per day; Group 3, woman smoking at the time of the

IVF treatment at least 9 cigarettes per day; Group 4, active smokers of 10 to 19 cigarettes per day; and Group 5, smokers of 20 or more cigarettes per day.

## REFERENCES

1. Mascarenhas, M. N., Flaxman, S. R., Boerma, T., Vanderpoel, S. & Stevens, G. A. National, Regional, and Global Trends in Infertility Prevalence Since 1990: A Systematic Analysis of 277 Health Surveys. *PLoS Med.* (2012). doi:10.1371/journal.pmed.1001356
2. De Geyter, C. Assisted reproductive technology: Impact on society and need for surveillance. *Best Pract. Res. Clin. Endocrinol. Metab.* **33**, 3–8 (2019).
3. Adamson, G. *et al.* International Committee for Monitoring Assisted Reproductive Technology: world report on assisted reproductive technology, 2016. (2020).
4. Adamson, G. D. *et al.* International Committee for Monitoring Assisted Reproductive Technology: world report on assisted reproductive technology, 2011. *Fertil. Steril.* **110**, 1067–1080 (2018).
5. Kasius, A. *et al.* Endometrial thickness and pregnancy rates after IVF: A systematic review and meta-analysis. *Hum. Reprod. Update* **20**, 530–541 (2014).
6. Lebovitz, O. & Orvieto, R. Treating patients with ‘thin’ endometrium-an ongoing challenge. *Gynecol. Endocrinol.* **30**, 409–414 (2014).
7. Margalioth, E. J., Ben-Chetrit, A., Gal, M. & Eldar-Geva, T. Investigation and treatment of repeated implantation failure following IVF-ET. *Hum. Reprod.* **21**, 3036–3043 (2006).
8. Roberts, S. A., Hann, M. & Brison, D. R. Factors affecting embryo viability and uterine receptivity: insights from an analysis of the UK registry data. *Reprod. Biomed. Online* **32**, 197–206 (2016).
9. Alpha and ESHRE. The Istanbul consensus workshop on embryo assessment: proceedings of an expert meeting † Alpha Scientists in Reproductive Medicine and ESHRE Special Interest Group of Embryology. *Hum. Fertil.* **26**, 1270–1283 (2011).
10. Nel-Themaat, L. & Nagy, Z. P. A review of the promises and pitfalls of oocyte and embryo metabolomics. *Placenta* **32**, S257–S263 (2011).
11. Botros, L., Sakkas, D. & Seli, E. Metabolomics and its application for non-invasive embryo assessment in IVF. *Mol. Hum. Reprod.* **14**, 679–690 (2008).
12. Katz-Jaffe, M. G. & McReynolds, S. Embryology in the era of proteomics. in *Fertility and Sterility* **99**, 1073–1077 (2013).
13. Andersen, A. N. *et al.* Assisted reproductive technology in Europe, 2004: results generated from European registers by ESHRE. *Hum. Reprod.* **23**, 756–771 (2008).
14. Paternot, G. *et al.* Intra- and interobserver analysis in the morphological assessment of early stage embryos during an IVF procedure: A multicentre study. *Reprod. Biol. Endocrinol.* **9**, 1–5 (2011).
15. Matson, P. L. Internal quality control and external quality assurance in the IVF laboratory. *Hum. Reprod.* **13**, 156–165 (1998).
16. Harper, J. *et al.* Adjuncts in the IVF laboratory: Where is the evidence for ‘add-

- on' interventions? *Hum. Reprod.* **32**, 485–491 (2017).
17. Lu, M. man *et al.* Trophoctoderm biopsy reduces the level of serum  $\beta$ -human chorionic gonadotropin in early pregnancy. *Fertil. Steril.* (2020). doi:10.1016/j.fertnstert.2020.05.015
  18. Gordon, C. E. & Racowsky, C. Trophoctoderm biopsy—perhaps not such a benign intervention. *Fertil. Steril.* 1–2 (2020). doi:10.1016/j.fertnstert.2020.06.027
  19. Penzias, A. *et al.* The use of preimplantation genetic testing for aneuploidy (PGT-A): a committee opinion. *Fertil. Steril.* **109**, 429–436 (2018).
  20. Rosenwaks, Z. *et al.* The pros and cons of preimplantation genetic testing for aneuploidy: clinical and laboratory perspectives. *Fertil. Steril.* **110**, 353–361 (2018).
  21. Leese, H. J. Metabolism of the preimplantation embryo: 40 years on. *Reproduction* **143**, 417–427 (2012).
  22. Renard, J. P., Philippon, A. & Menezo, Y. In-vitro uptake of glucose by bovine blastocysts. *Reproduction* **58**, 161–164 (1980).
  23. Seli, E. *et al.* Noninvasive metabolomic profiling of embryo culture media using Raman and near-infrared spectroscopy correlates with reproductive potential of embryos in women undergoing in vitro fertilization. *Fertil. Steril.* **88**, 1350–1357 (2007).
  24. Sakkas, D. Embryo selection using metabolomics. *Methods Mol. Biol.* **1154**, 533–540 (2014).
  25. Ballin, N. Z. & Laursen, K. H. To target or not to target? Definitions and nomenclature for targeted versus non-targeted analytical food authentication. *Trends Food Sci. Technol.* **86**, 537–543 (2019).
  26. Bracewell-Milnes, T. *et al.* Metabolomics as a tool to identify biomarkers to predict and improve outcomes in reproductive medicine: A systematic review. *Hum. Reprod. Update* **23**, 723–736 (2017).
  27. Ahlström, A. *et al.* Cross-validation and predictive value of near-infrared spectroscopy algorithms for day-5 blastocyst transfer. *Reprod. Biomed. Online* **22**, 477–484 (2011).
  28. Hardarson, T. *et al.* Non-invasive metabolomic profiling of Day 2 and 5 embryo culture medium: A prospective randomized trial. *Hum. Reprod.* **27**, 89–96 (2012).
  29. Sfontouris, I. *et al.* Non-invasive metabolomic analysis using a commercial NIR instrument for embryo selection. *J. Hum. Reprod. Sci.* **6**, 133 (2013).
  30. Seli, E. *et al.* Noninvasive metabolomic profiling as an adjunct to morphology for noninvasive embryo assessment in women undergoing single embryo transfer. *Fertil. Steril.* (2010). doi:10.1016/j.fertnstert.2009.03.078
  31. Vergouw, C. G. *et al.* Day 3 embryo selection by metabolomic profiling of culture medium with near-infrared spectroscopy as an adjunct to morphology: A randomized controlled trial. *Hum. Reprod.* **27**, 2304–2311 (2012).
  32. Vergouw, C. G. *et al.* Metabolomic profiling by near-infrared spectroscopy as a tool to assess embryo viability: a novel, non-invasive method for embryo selection. *Hum. Reprod.* **23**, 1499–1504 (2008).
  33. Sakkas, D., Botros, L., Henson, M., Judge, K. & Roos, P. Metabolomics: The ViaMetrics-E<sup>TM</sup> Procedure for Assessing Embryo Viability. in *Practical Manual of In Vitro Fertilization* 405–412 (2012). doi:10.1007/978-1-4419-1780-5
  34. Brison, D. R., Hollywood, K., Arnesen, R. & Goodacre, R. Predicting human

- embryo viability: The road to non-invasive analysis of the secretome using metabolic footprinting. *Reprod. Biomed. Online* **15**, 296–302 (2007).
35. Grunert, T., Stephan, R., Ehling-Schulz, M. & Jöhler, S. Fourier Transform Infrared Spectroscopy enables rapid differentiation of fresh and frozen/thawed chicken. *Food Control* **60**, 361–364 (2016).
  36. Rodriguez-Saona, L. E., Giusti, M. M. & Shotts, M. Advances in infrared spectroscopy for food authenticity testing. in *Advances in food authenticity testing* 71–116 (2016). doi:10.1016/B978-0-08-100220-9.00004-7
  37. Kosa, G. *et al.* Assessment of the scalability of a microtiter plate system for screening of oleaginous microorganisms. *Appl. Microbiol. Biotechnol.* **102**, 4915–4925 (2018).
  38. Sellick, C. A. *et al.* Rapid monitoring of recombinant antibody production by mammalian cell cultures using Fourier transform infrared spectroscopy and chemometrics. *Biotechnol. Bioeng.* **106**, 432–442 (2010).
  39. Musmann, C., Joeris, K., Markert, S., Solle, D. & Scheper, T. Spectroscopic methods and their applicability for high-throughput characterization of mammalian cell cultures in automated cell culture systems. *Eng. Life Sci.* **16**, 405–416 (2016).
  40. Scholz, T., Lopes, V. V. & Calado, C. R. C. High-throughput analysis of the plasmid bioproduction process in *Escherichia coli* by FTIR spectroscopy. *Biotechnol. Bioeng.* **109**, 2279–2285 (2012).
  41. Bağcıoğlu, M., Fricker, M., Jöhler, S. & Ehling-Schulz, M. Detection and identification of *Bacillus cereus*, *Bacillus cytotoxicus*, *Bacillus thuringiensis*, *Bacillus mycoides* and *Bacillus weihenstephanensis* via machine learning based FTIR spectroscopy. *Front. Microbiol.* **10**, 1–10 (2019).
  42. Vogt, S. *et al.* Fourier-Transform Infrared (FTIR) Spectroscopy for Typing of Clinical *Enterobacter cloacae* Complex Isolates. *Front. Microbiol.* **10**, 1–11 (2019).
  43. Depciuch, J. *et al.* FTIR Spectroscopy of Cerebrospinal Fluid Reveals Variations in the Lipid: Protein Ratio at Different Stages of Alzheimer’s Disease. *J. Alzheimer’s Dis.* **68**, 281–293 (2019).
  44. Blat, A. *et al.* Fourier transform infrared spectroscopic signature of blood plasma in the progression of breast cancer with simultaneous metastasis to lungs. *J. Biophotonics* **12**, 1–11 (2019).
  45. Untereiner, V. *et al.* Bile analysis using high-throughput FTIR spectroscopy for the diagnosis of malignant biliary strictures: A pilot study in 57 patients. *J. Biophotonics* **7**, 241–253 (2014).
  46. Wenning, M. & Scherer, S. Identification of microorganisms by FTIR spectroscopy: perspectives and limitations of the method. *Appl. Microbiol. Biotechnol.* **97**, 7111–7120 (2013).
  47. Ollesch, J. *et al.* It’s in your blood: Spectral biomarker candidates for urinary bladder cancer from automated FTIR spectroscopy. *J. Biophotonics* **7**, 210–221 (2014).
  48. Zhang, X. *et al.* Profiling serologic biomarkers in cirrhotic patients via high-throughput Fourier transform infrared spectroscopy: Toward a new diagnostic tool of hepatocellular carcinoma. *Transl. Res.* **162**, 279–286 (2013).
  49. Peuchant, E. *et al.* Infrared spectroscopy: a reagent-free method to distinguish Alzheimer’s disease patients from normal-aging subjects. *Transl. Res.* **152**, 103–112 (2008).
  50. Lacombe, C. *et al.* Rapid screening of classic galactosemia patients: A proof-

- of-concept study using high-throughput FTIR analysis of plasma. *Analyst* **140**, 2280–2286 (2015).
51. Scott, D. A. *et al.* Diabetes-related molecular signatures in infrared spectra of human saliva. *Diabetol. Metab. Syndr.* **2**, 48 (2010).
  52. Bosch, A. *et al.* Fourier transform infrared spectroscopy for rapid identification of nonfermenting gram-negative bacteria isolated from sputum samples from cystic fibrosis patients. *J. Clin. Microbiol.* **46**, 2535–2546 (2008).
  53. Lasch, P. *et al.* Antemortem Identification of Bovine Spongiform Encephalopathy from Serum Using Infrared Spectroscopy. *Anal. Chem.* **56**, 6673–6678 (2002).
  54. Fabian, H., Lasch, P. & Naumann, D. Analysis of biofluids in aqueous environment based on mid-infrared spectroscopy. *J. Biomed. Opt.* **10**, 031103 (2005).
  55. Kosa, G., Shapaval, V., Kohler, A. & Zimmermann, B. FTIR spectroscopy as a unified method for simultaneous analysis of intra- and extracellular metabolites in high-throughput screening of microbial bioprocesses. *Microb. Cell Fact.* **16**, 1–11 (2017).
  56. Baker, M. J. *et al.* Developing and Understanding Biofluid Vibrational Spectroscopy: A Critical Review. *Chem. Soc. Rev.* **45**, 1803–1818 (2016).
  57. Baker, M. J. *et al.* Clinical applications of infrared and Raman spectroscopy: State of play and future challenges. *Analyst* **143**, 1735–1757 (2018).
  58. Lasch, P. & Naumann, D. *Infrared Spectroscopy in Microbiology*. *Encyclopedia of Analytical Chemistry* (2015). doi:10.1002/9780470027318.a01117.pub2
  59. Petibois, C., Melin, A. M., Perromat, A., Cazorla, G. & Délérès, G. Glucose and lactate concentration determination on single microsamples by Fourier-transform infrared spectroscopy. *J. Lab. Clin. Med.* **135**, 210–215 (2000).
  60. Hackett, M. J. *et al.* Concurrent glycogen and lactate imaging with FTIR spectroscopy to spatially localize metabolic parameters of the glial response following brain ischemia. *Anal. Chem.* **88**, 10949–10956 (2016).
  61. Kohler, A. *et al.* High-throughput biochemical fingerprinting of *Saccharomyces cerevisiae* by Fourier transform infrared spectroscopy. *PLoS One* **10**, 1–22 (2015).
  62. Wold, S. & Sjöström, M. SIMCA: A Method for Analyzing Chemical Data in Terms of Similarity and Analogy. in 243–282 (1977). doi:10.1021/bk-1977-0052.ch012
  63. Gardner, D. K., Wela, P. & Wale, P. L. Analysis of metabolism to select viable human embryos for transfer. *Fertil. Steril.* **99**, 1062–1072 (2013).
  64. Dubey, P. K., Tripathi, A. & Ali, A. Assisted Reproductive Technologies in Infertility Treatment: Opportunities and Challenges. in *Male Infertility: Understanding, Causes and Treatment* (eds. Singh, R. & Singh, K.) 481–497 (Springer Singapore, 2017). doi:10.1007/978-981-10-4017-7
  65. Vahlsing, T., Delbeck, S., Leonhardt, S. & Heise, H. M. Noninvasive Monitoring of Blood Glucose Using Color-Coded Photoplethysmographic Images of the Illuminated Fingertip Within the Visible and Near-Infrared Range: Opportunities and Questions. *J. Diabetes Sci. Technol.* **12**, 1169–1177 (2018).
  66. Zhang, S. *et al.* Nondestructive Measurement of Hemoglobin in Blood Bags Based on Multi-Pathlength VIS-NIR Spectroscopy. *Sci. Rep.* **8**, 1–9 (2018).
  67. Sakudo, A. Near-infrared spectroscopy for medical applications: Current status

- and future perspectives. *Clin. Chim. Acta* **455**, 181–188 (2016).
68. Seli, E., Robert, C. & Sirard, M. A. Omics in assisted reproduction: Possibilities and pitfalls. *Mol. Hum. Reprod.* **16**, 513–530 (2010).
  69. Bosch, A. *et al.* Rapid discrimination of lactobacilli isolated from kefir grains by FT-IR spectroscopy. *Int. J. Food Microbiol.* **111**, 280–287 (2006).
  70. Elder, K. & Dale, B. *In-Vitro Fertilization*. (Cambridge University Press, 2019). doi:10.1017/9781108611633
  71. Velde T. & Pearson P. L. The variability of female reproductive aging. *Hum. Reprod. Update* **8**, 141–154 (2002).
  72. Albertini, D. F. *et al.* A prognosis-based approach to infertility: understanding the role of time. *Hum. Reprod.* **32**, 1556–1559 (2017).
  73. Van Kooij, R. J., Looman, C. W. N., Habbema, J. D. F., Dorland, M. & Te Velde, E. R. Age-dependent decrease in embryo implantation rate after in vitro fertilization. *Fertil. Steril.* **66**, 769–775 (1996).
  74. Chuang, C.-C. *et al.* Age is a better predictor of pregnancy potential than basal follicle-stimulating hormone levels in women undergoing in vitro fertilization. *Fertil. Steril.* **79**, 63–68 (2003).
  75. Sharif, K., Elgendy, M., Lashen, H. & Afnan, M. Age and basal follicle stimulating hormone as predictors of in vitro fertilisation outcome. *BJOG An Int. J. Obstet. Gynaecol.* **105**, 107–112 (1998).
  76. Padilla, S. L. & Garcia, J. E. Effect of maternal age and number of in vitro fertilization procedures on pregnancy outcome. *Fertil. Steril.* **52**, 270–273 (1989).
  77. Van Voorhis, B. J. In Vitro Fertilization. *N. Engl. J. Med.* **356**, 379–386 (2007).
  78. Hart, R. J. Physiological Aspects of Female Fertility: Role of the Environment, Modern Lifestyle, and Genetics. *Physiol. Rev.* **96**, 873–909 (2016).
  79. Palermo, G., Joris, H., Devroey, P. & Van Steirteghem, A. C. Pregnancies after intracytoplasmic injection of single spermatozoon into an oocyte. *Lancet* **340**, 17–18 (1992).
  80. Van Steirteghem, A. C. *et al.* High fertilization and implantation rates after intracytoplasmic sperm injection. *Hum. Reprod.* **8**, 1061–1066 (1993).
  81. Penzias, A. *et al.* Performing the embryo transfer: a guideline. *Fertil. Steril.* **107**, 882–896 (2017).
  82. Lasch, P. Spectral pre-processing for biomedical vibrational spectroscopy and microspectroscopic imaging. *Chemom. Intell. Lab. Syst.* **117**, 100–114 (2012).
  83. Helm, D. & Naumann, D. Identification of some bacterial cell components by FT-IR spectroscopy. *FEMS Microbiol. Lett.* **126**, 75–79 (1995).
  84. Rebuffo-Scheer, C. A., Dietrich, J., Wenning, M. & Scherer, S. Identification of five *Listeria* species based on infrared spectra (FTIR) using macrosamples is superior to a microsample approach. *Anal. Bioanal. Chem.* **390**, 1629–1635 (2008).
  85. Helm, D. *et al.* Classification and identification of bacteria by Fourier-transform infrared spectroscopy. *J. Gen. Microbiol.* **137**, 69–79 (1991).
  86. Zontov, Y. V., Rodionova, O. Y., Kucheryavskiy, S. V. & Pomerantsev, A. L. DD-SIMCA – A MATLAB GUI tool for data driven SIMCA approach. *Chemom. Intell. Lab. Syst.* **167**, 23–28 (2017).
  87. Cavelaars, M. *et al.* OpenClinica. *J. Clin. Bioinforma.* **5**, S2 (2015).



## **ACKNOWLEDGEMENTS**

This research was supported by a Merck Serono award, "Grant for Fertility Innovation" GFI-2012-1; by an award from Comisión de Investigaciones Científicas de la Provincia de Buenos Aires, (CIC-PBA), "PREMIO CIENCIA Y COMUNIDAD 2013"; by an award from Ministerio de Ciencia, Tecnología e Innovación Productiva (MINCyT), "PREMIO INNOVAR 2015"; and from a grant of the Fondo para la Investigación Científica y Tecnológica (FONCYT), ANR-800-183/11. C.B.F. was supported by CONICET, Argentina; A.B was supported by CIC PBA. Dr. Donald F. Haggerty, a retired academic career investigator and native English speaker, edited the final version of the manuscript.

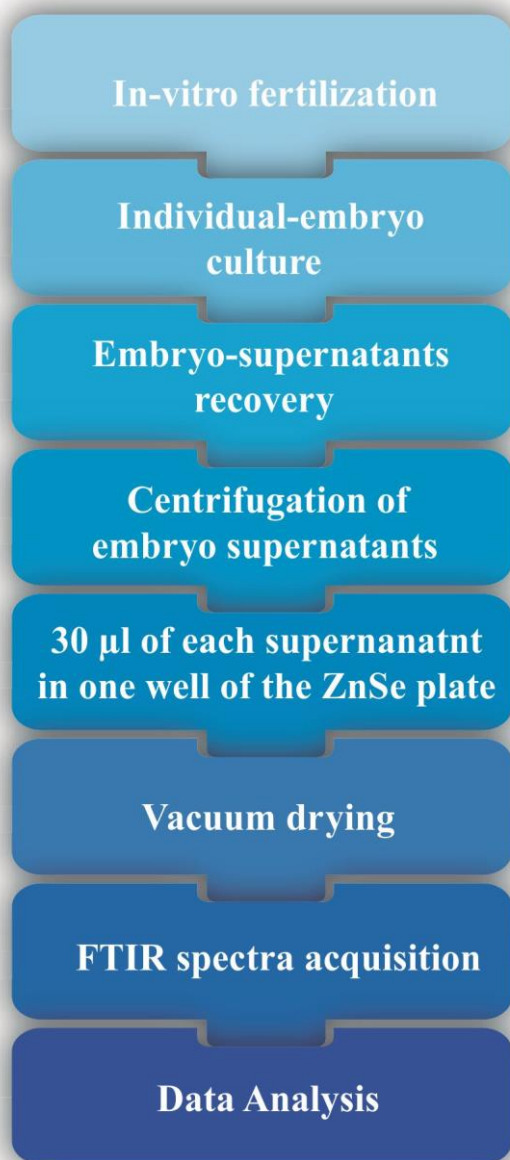
## **AUTHOR CONTRIBUTIONS**

C.B.F., M.G., C.B., P.L., J.S., A.K., V.T., V.S., and A.B designed the experiments, supervised research, and wrote and edited the paper. O.M.Y., M.H. and A.B. supervised the project. F.A. and L.G. organized and oversaw the clinical data collection. M.G.P. and C.B. collected embryo culture supernatants and oversaw the sample collection. A.K., V.S., V. T., C.B.F., and A.B. devised and implemented the mathematical models and statistical analyses. All the authors discussed the results and implications.

## **COMPETING INTERESTS**

The authors declare no competing interests.

Correspondence and requests for materials should be addressed to A.B.

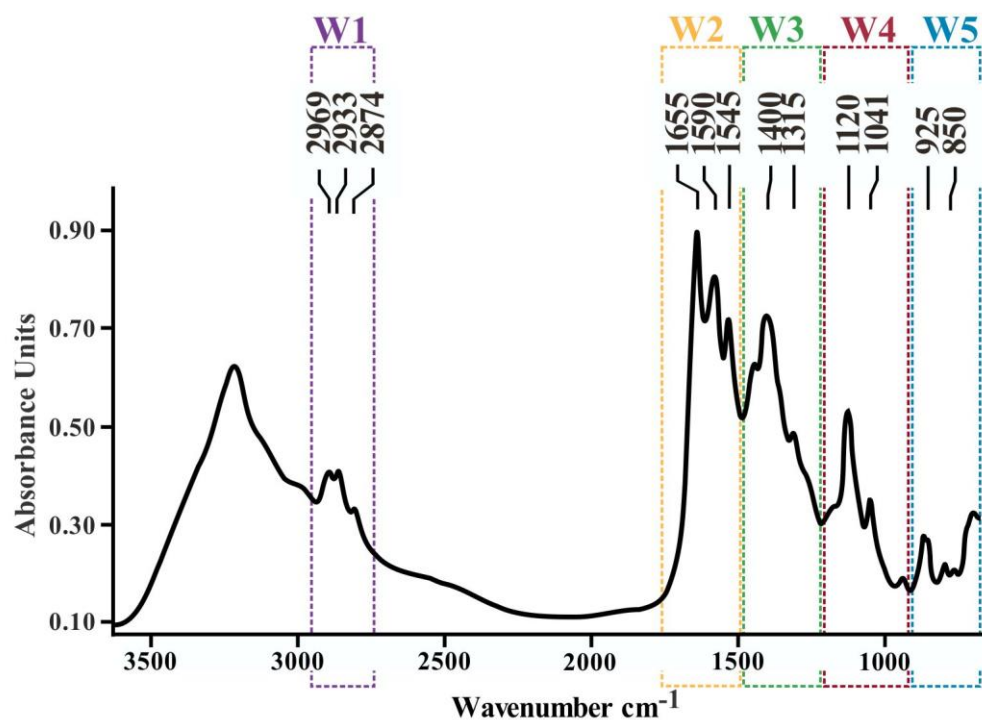


922

923 **Fig. 1. Flow sheet of the standardized approach for FTIR spectral measurements**

924 **of embryo supernatant**

a



b

Spectral windows (cm-1)		Wavenumber (cm-1)	Band assignment <sup>1</sup>
W1 2800-3000	Aliphatic chains	2969 2933 2874	$\nu_{as}$ CH <sub>3</sub> $\nu_{as}$ CH <sub>2</sub> $\nu_s$ CH <sub>3</sub>
W2 1500-1800	Proteins and Peptides	1655 1590 1545	$\nu$ >C=O and $\delta$ C-N $\delta$ N-H $\delta$ N-H and $\nu$ C-N
W3 1200-1500	Mixed region	1400 1,315	$\nu$ -COO $\nu$ C-N and $\delta$ N-H
W4 900-1200	Carbohydrate	1120 1041	$\nu$ C-O
W5 650-900	Fingerprint region	925 850	$\nu$ O-H out of plane $\nu_s$ C-O-C

**Fig. 2. Spectral description of embryo-culture supernatants.** Panel a: FTIR spectrum of a 3-day-embryo supernatant recovered from the culture of an embryo of class IMP. The main spectral windows (W1 to W5) indicated above the figure correspond to: W1 aliphatic chains, (2800–3000 cm<sup>-1</sup>), W2 the region assigned to protein absorptions (1500–1800 cm<sup>-1</sup>), W3 the mixed region (1200–1500 cm<sup>-1</sup>), W4

the region assigned to carbohydrate-absorption bands (900–1200  $\text{cm}^{-1}$ ), and W5 the fingerprint region (650–900  $\text{cm}^{-1}$ ).  $\nu$  = stretching vibrations,  $s$  = symmetric vibrations, and  $as$  = antisymmetric vibrations,  $\delta$  = bending. Panel b: Spectral windows associated with functional groups in biomolecules and the band assignments for the 3-day-embryo supernatants.

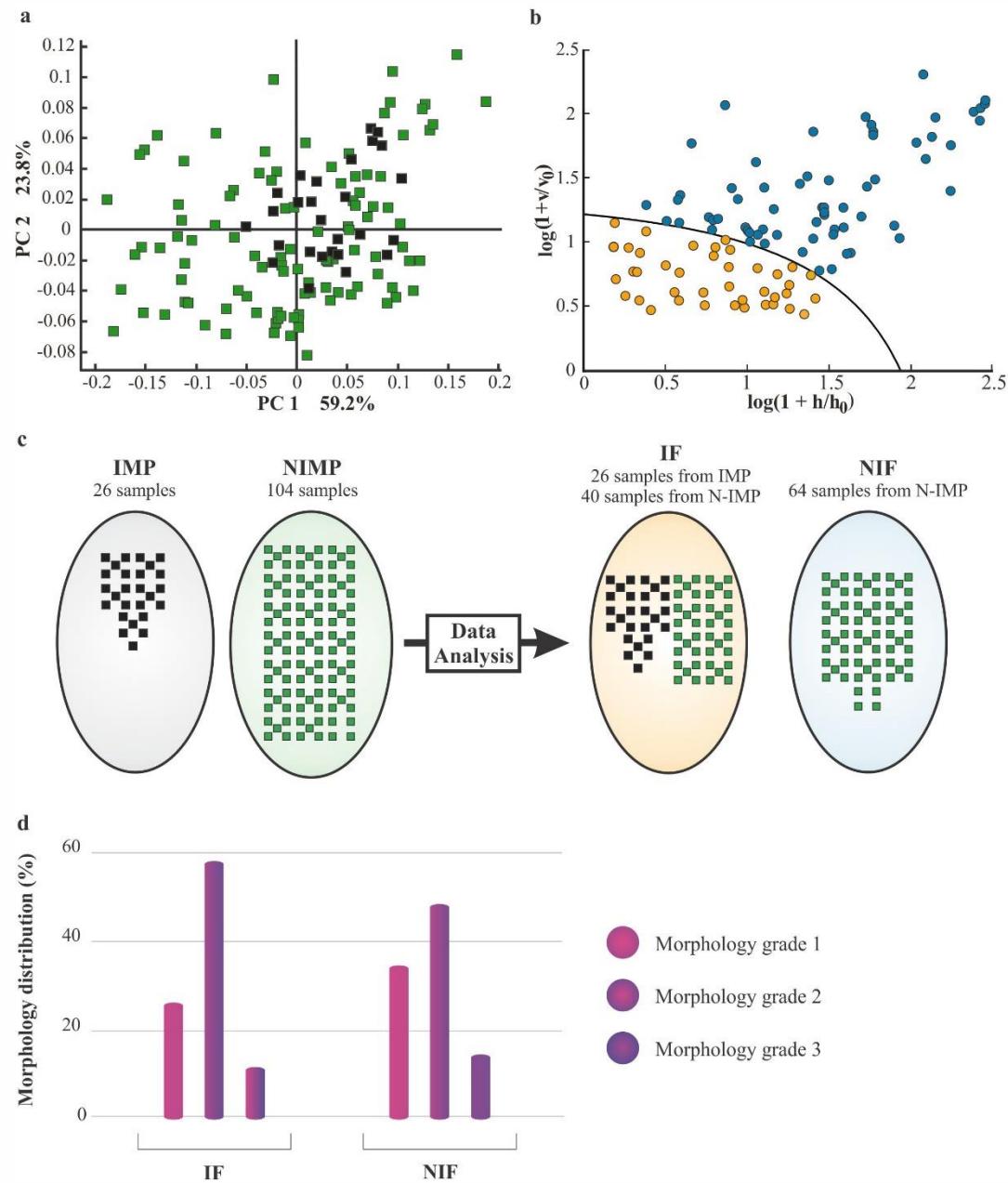


**Fig. 3. Metabolomics study of embryos based on FTIR spectroscopy in combination with multivariate analyses.** Panel a: PCA-score plot based on FTIR metabolic fingerprinting of embryo-culture supernatants. Black squares, class IMP, (spectra of supernatants from embryos that implanted at 100%); green squares, class NIMP (spectra of supernatants for embryos that did not implant at 0% implantation). Panel b: Classification of the results for class-NIMP data by SIMCA modelling. Orange dots, class IF (implantation fingerprinting); blue dots, class NIF (nonimplantation fingerprinting). Panel c: Logic diagram indicating the distribution of samples according to the implantation outcomes (IMP *versus* NIMP) and their assignment to the IF or NIF groups according to the results obtained by the PCA and SIMCA analyses. The IF group comprises all the IMP spectra (26 samples) and a fraction of the NIMP spectra with features of the metabolic implantation fingerprint (40 samples), while the NIF group contains nonimplantation fingerprints from the NIMP spectra (64 samples). Panel d: Distribution of embryo-morphology qualities as determined by the Istanbul consensus within the IF and NIF groups (morphology grade 1, morphology grade 2, morphology grade 3). The percent distribution of the different morphological grades is plotted on the *ordinate* for the two metabolomic classes indicated on the *abscissa*. The statistical analysis revealed no significant differences between the embryo-morphology grades observed with the IF and the NIF patterns ( $p = 0.125$ ).

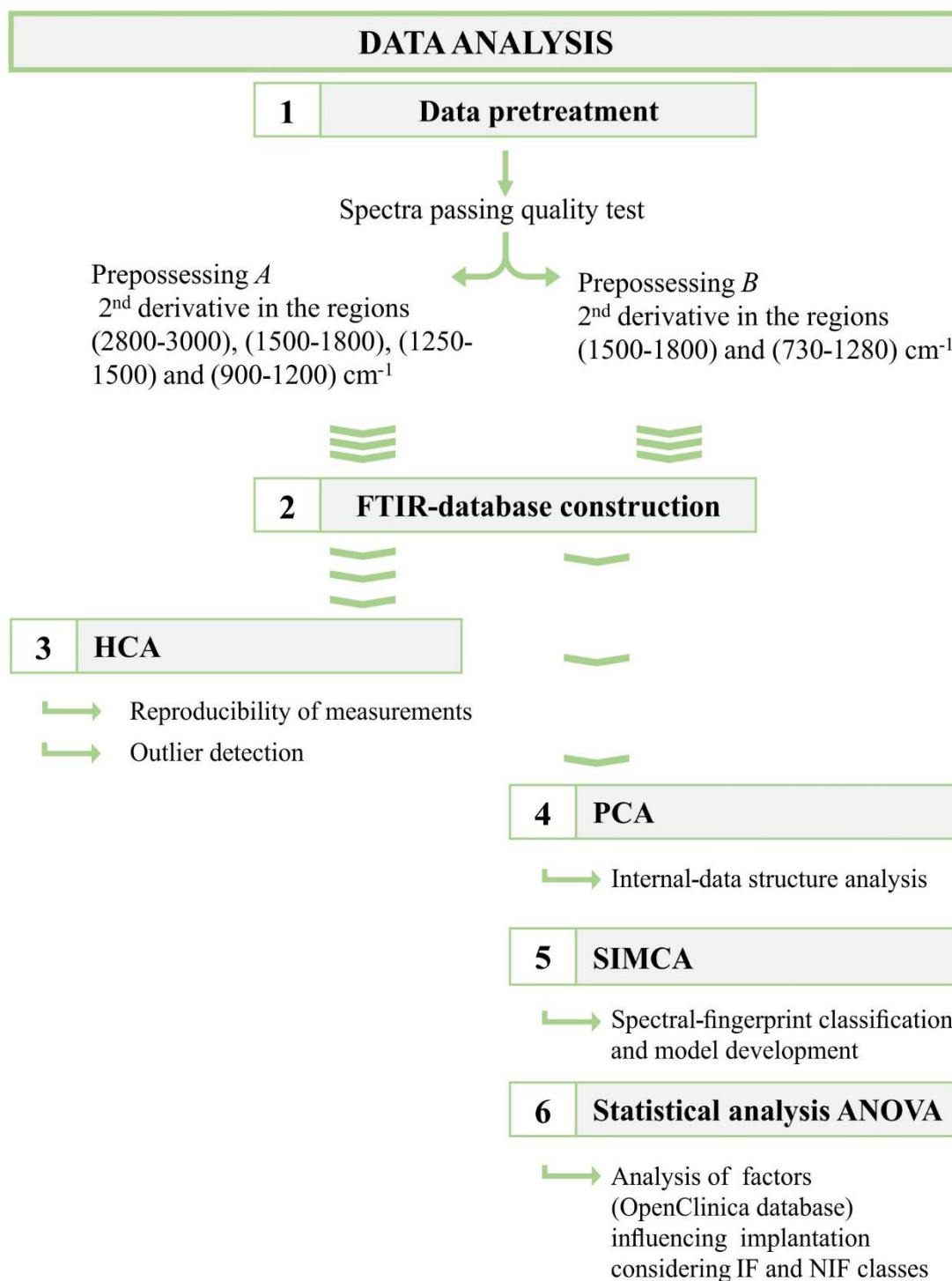
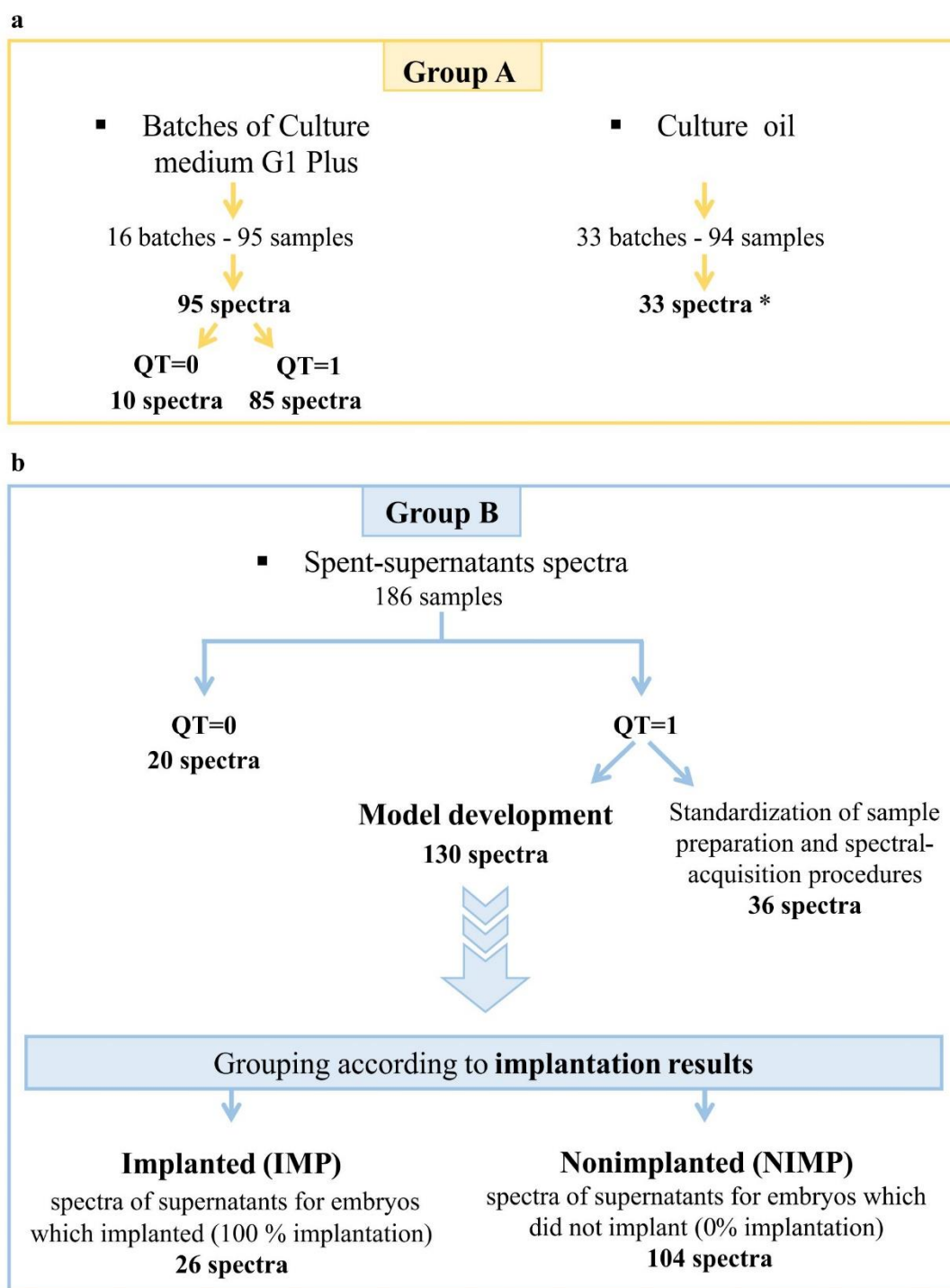


**Fig. 4. FTIR-spectral–data-analysis flow chart for embryo supernatants.**



968 were transferred to patients, indicating the embryos that implanted and those that  
969 failed to do so along with the quality-testing results of the corresponding sample  
970 groups (Group B). The bottom window of Panel b summarizes the spectra of the  
971 supernatants associated with the different outcomes of the embryo transfers for  
972 implantation, indicated by implantation (IMP) and nonimplantation (NIMP)  $QT = 1$ ,  
973 fulfilled the spectral-quality requirements,  $QT = 0$  did not meet the spectral-quality  
974 requirements.

975 \*Only one sample from each batch was measured.